Design of Double Y Branch Waveguide in Acceleration Seismic Geophone

De En
School of Electrical Engineering and Automation, Henan Polytechnic University,
Jiaozuo, China
Email: ende@hpu.edu.cn

Jieyu Feng, Ningbo Zhang, Ningning Wang, Xiaobin Wang
School of Electrical Engineering and Automation, Henan Polytechnic University,
Jiaozuo, China
Email: jieyumujin@163.com, mazhutianxia@163.com

***Abstract*—Dual M-Z interferometer is the sensitive element of three-component acceleration seismic geophone, while Y branch waveguide is the basic optical components composed of dual M-Z interferometer, so the design of Y branch waveguide directly affects the performance of three-component acceleration seismic geophone. Firstly, branch waveguide and S-shaped bent waveguide are introduced, and symmetrical double Y branch S-shaped bent waveguide is designed based on this. Secondly, the bending loss of the branch waveguide is analyzed and calculated. The transmission of 1/2Y branch waveguide and 1/4Y branch waveguide , and the bending loss changes with the length of 1/2Y branch waveguide and 1/4Y branch waveguide is simulated by MATLAB. The result shows that the maximum bending loss of 1/2 Y branch waveguide is the 0.156dB, and the bending loss is close to 0 after *L*>320μm; the maximum bending loss of 1/4 Y branch waveguide is 0.058dB, and the bending loss is close to 0 after *L*>200μm. The design of double Y branch meets the requirement of low loss. Thirdly, the optical power conversion of branch waveguide in 3dB coupler is simulated and analyzed. Finally, proton exchange and Ti diffusion technique are compared; the advantages of proton exchange technology are summarized; the principle of proton exchange is introduced; and a good proton exchange annealing condition is summarized.**

***Index items*—acceleration; photoelastic waveguide; 3dB coupler; dual M-Z interferometer**

I. INTRODUCTION

With the rapid development of three-component seismic exploration technology, in order to prove complex geological environment and identify the reservoir of oil and gas fields to increase the recoverable reserves, the performance of three-component acceleration seismic geophone that receives the seismic signals is essential to the whole seismic record and the interpretation of seismic data.

As the optical waveguide has the advantages of light weight, anti-electromagnetic interference, etc., in recent years, a lot of sensing technologies testing acceleration based on the theory of photoelastic waveguide are carried out at home and abroad. Some typical representatives are: (1)The photoelastic crystal is used to sense acceleration, which causes the refractive index changes of the crystal, and then acceleration is detected by detecting the light phase changes of photoelastic crystal; (2)The weight is put on a thin photoelastic crystal to sense acceleration, which results in the sheet deformation and causes the changes of light phase through the crystal; (3)The double photoelastic layers with reflection surface are used to sense the acceleration, and the CCD technology is used to playback the phase changes to cause the photoelastic changes.

II. PHOTOELASTIC EFFECT

The media body will produce stress under external force, and the microscopic particles composed of medium occurs displacement, resulting in strain, which will lead to the changes in polarization properties of the medium (or dielectric constant), and the final performance is the refractive index changes. The external force leads to the elastic deformation of media, thereby causing a change in the refractive index of media. The phenomenon is known as the photoelastic effect, which is also known as birefringence or mechanical stress birefringence [1]. When a transparent isotropic medium subjected to mechanical stress, the media will become the optical anisotropic media. When stress exists in the internal of the material, the stress changes the refractive index of the optical waveguide through photo-elastic effect, causing the birefringence of waveguide, thus affecting the performance of optical waveguide devices.

$LiNbO_3$ crystal is a piezoelectric, ferroelectric and electro-optical crystal, and it belongs to the trigonal system negative uniaxial crystal. $LiNbO_3$ crystal has many important applications in key technologies, such as micro-acoustic devices, high-frequency high-temperature transducers, infrared detectors, laser modulation, laser frequency doubling, optical parametric oscillators, radio frequency filters and waveguides, which is a very common application piezoelectric, ferroelectric and electro-optic crystal [2].

doi:10.4304/jcp.8.1.217-224

The sensitive element of three-component acceleration seismic geophone——dual M-Z interferometer is the core of achieving the right detection of acceleration of three-component acceleration seismic geophone. Y branch waveguide is the basic optical component composed of dual M-Z interferometer, so the design of Y branch waveguide directly affects the performance of three-component acceleration seismic geophone.

In order to correctly detect the external acceleration, it needs to make strip waveguides on the $LiNbO_3$ substrate of three-component acceleration seismic geophone, which converts the change in the external acceleration to a phase change within the optical waveguides. Common optical waveguides include the curved waveguide with the ability to change the direction of light path and the branch waveguides synthesizing and separating the optical power. Y-branch waveguides in the structure of dual M-Z interferometer is the power unit and power sharing unit of 3dB coupler.

III. The Basic Principal Of M-Z Interferometer

M-Z interferometer is a two-beam interferometer, and its structural schematic diagram is shown in Fig.1. Coherent light emitted by the laser is sent into the two arms of M-Z interferometer respectively after passing through the polarizer, while one arm is a reference arm, and another arm is the signal arm. Two beams of laser that outputs from the two arms produce interference effects after overlapping, and the separating beam and synthesizing beam used for the interferometer are achieved by two 3dB directional coupler. After interference, the signal beam transmitted to the photodetector to convert to electrical signals through the optical waveguides, and the parameters to be measured are gotten by the process of relevant signal processing system. Its anti-interference ability can be strengthened by using two 3dB directional coupler to achieve synthesizing and separating beams [3].

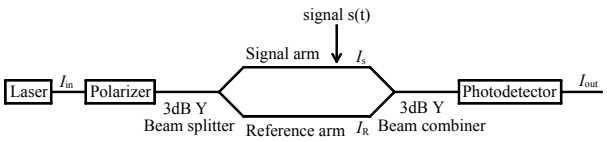

Fig.1. Schematic diagram of M-Z interferometer

It can seen from the two-beam interference principle that the optical field amplitudes output from the reference arm and the signal arm respectively are

$$A_r = A_0\sqrt{\alpha_r K_1 K_2}\cos(\omega_0 t + \varphi_r) \tag{1}$$

$$A_s = A_0\sqrt{\alpha_s (1-K_1)(1-K_2)}\cos(\omega_0 t + \varphi_s) \tag{2}$$

Where, A_r, A_s respectively are the amplitudes of the optical field of the reference arm and the signal arm; A_0 is the optical field amplitude of the input of the interferometer; α_s, φ_s, α_r, φ_r respectively are the optical loss and phase delay of the signal arm and the reference arm; K_1, K_2 are the power coupling coefficients of the two fiber coupler. When the two beams of light superposes, the intensity is

$$I = (A_r + A_s)^2 \tag{3}$$

Substitute A_r, A_s into the above equation, there

$$I = I_0\{\alpha_r K_1 K_2 + \alpha_s (1-K_1)(1-K_2) + 2\sqrt{\alpha_r \alpha_s K_1 K_2 (1-K_1)(1-K_2)}\cos(\varphi_r - \varphi_s)\} \tag{4}$$

Where, I_0 is the optical intensity of the light output from the laser; α is the coupling coefficient; φ_s is the phase shift caused by the external signal.

The contrast ratio of output interference fringes γ is the quantitative description physical quantity for the ups and downs of the interference field strength.

$$\gamma = \frac{I_{max} - I_{min}}{I_{max} + I_{min}} \tag{5}$$

$$\begin{cases} I_{max} = I_1 + I_2 + 2\sqrt{I_1 I_2}, \text{when phase difference is } 2k\pi \\ I_{min} = I_1 + I_2 - 2\sqrt{I_1 I_2}, \text{when phase difference is } (2k+1)\pi \end{cases} \quad k = 0, \pm 1, \pm 2 \tag{6}$$

Where, I_{min}, I_{max} respectively are the maximum value and minimum value actually observed in the interference field; I_1, I_2 respectively are the light intensity of two arms. The difference of I_{min} and I_{max} is only determined by the field intensity of coherent light, but I_{min} and I_{max} are not only the field intensity of coherent light, but also include the field intensity of non-coherent light. So the composition of non-coherent light should be suppressed as much as possible.

When designing the M-Z interferometer, narrow width spectral line, stable frequency, and good performance single-longitudinal mode laser should be chosen as the light source. When producing the M-Z interferometer, the splitting ratio of 1×2 directional coupler should be strictly implemented in accordance with 3dB targets in order to ensure outputting stable detection signal, high signal to noise ratio and high detection sensitivity.

IV. Branch Waveguide

The two basic structures of branch waveguide are symmetry two branch waveguide and of asymmetric two branch waveguide. No matter what the shape of the branch waveguide, a tapered waveguide should be set in the front part of the branch point to reduce reflection and radiation loss and avoid creating new patterns of spread. Cone angle and the angle of branch arm are very small, typically a few tenths to 0.0 several times. In the 4μm wide single-mode symmetric two branch waveguide, (Fig. 2(a)), take θ=0.1047° and distribute power dividely, then the loss is about 1dB [4]. For the asymmetric branch waveguide (Fig. 2 (b)), the power distribution ratio can be adjusted by changing the branch angle. For the multi-branch waveguide (Fig. 2(c), (d)), it needs to change the width or the refractive index of each branch in order to achieve equal distribution of power and try to reduce the radiation loss, which is very difficult to implement. Thus, more symmetric two branch waveguide in series to form similar to 1×4 branch waveguide as shown in Fig. 2(d) in

the sensitive element of three-component acceleration seismic geophone.

(a)Symmetrical two branches

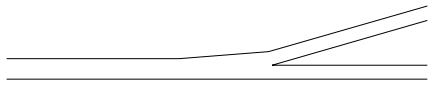

(b)Asymmetric two branches

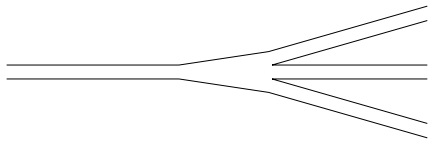

(c)Symmetrical three branches

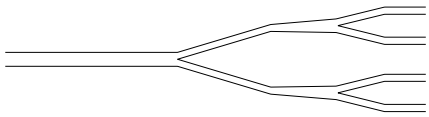

(d)1×4 branches

Fig.2 The basic structure of single-mode waveguide branches

The design uses a series of two symmetrical branch waveguides, because the method is more likely to control in the process, and there is no large ones to limit in principle.

V. S-SHAPED CURVED WAVEGUIDE

If Y-branch structure with a bent structure as shown in Fig. 3(a) is used, the radiation loss of two bending parts is large. To reduce the radiation loss, the angle θ should be reduced. But decrease the angle and achieve certain functions, it will inevitably lead to a significant increase in the length of the device, which is not conducive to miniaturization of the device and will bring some production difficulties. To reduce the radiation loss, and try to ensure the miniaturization of the device, S-bend waveguide as shown in Fig. 3(b) is used. For S-bend waveguide, a smooth curve waveguide composed by two circulars with the radius R_1 and R_2 are usually instead of the above bending waveguide. When two arcs overlap in the junction of tangent, the radiation loss can be minimized.

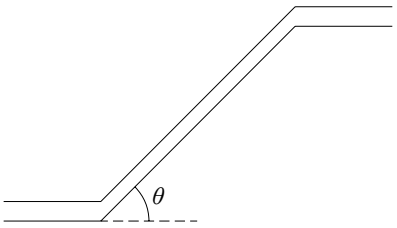

(a)Bent waveguide

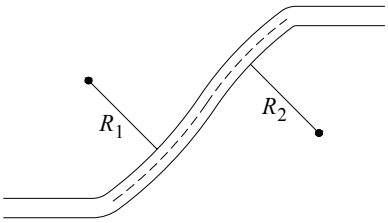

(b)S-bend waveguide

Fig.3 Waveguides with a bent structure

When designing Y branch, the key issue is how to reduce the power loss caused by phase and field mismatch at the branch. There are mainly two ways for the optimization of Y branch: change the shape of branch and change the refractive index distribution. Change the refractive index distribution. Because the production process is complicated and difficult to achieve, the method of changing the shape of the branch is used.

The shape of the branch is changed by adjusting the structural parameters which play a leading role in the transmission performance to Y branch waveguide to achieve the optimization of Y branches. In order to minimize the pure bending loss of S-shaped curved waveguide and the coupling loss generated by the emergence of two arcs with different radius, when the transition loss where the endpoints of S-shaped curved waveguide connected with straight waveguide is omitted, the performance of S-shaped curved waveguide is mainly determined by the bending length L, bending height h and branch angle θ three structural parameters, as shown in Fig. 4.

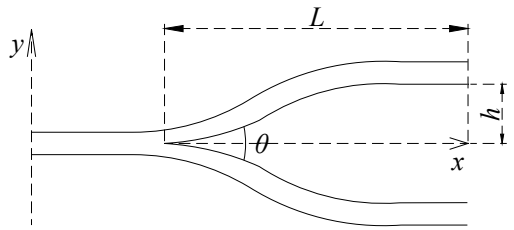

Fig. 4. Structure of Y-branch waveguide

Commonly used S-shaped curved waveguides are double arc type, increasing arcsine function and cosine function type. Sine function type waveguide is used, and the expression of S-shaped curved increasing arcsine function waveguide is

$$y(x) = \frac{h}{L}x - \frac{h}{2\pi}\sin(\frac{2\pi x}{L}) \tag{7}$$

The angle of Y branch waveguide is

$$\theta = 2\arctan\frac{h}{L} \tag{8}$$

VI. DESIGN OF STRUCTURE OF SYMMETRICAL DOUBLE Y-BRANCH S-SHAPED CURVED WAVEGUIDE

Considering the relationship of the splitting ratio and transmission loss, symmetrical double Y branch S-shaped

type bending waveguide in dual M-Z interferometer is designed, and its structure is shown in Fig.5. The structural parameters of 1/2 Y branch waveguide and 1/4 Y branch waveguide is shown in Table 1.

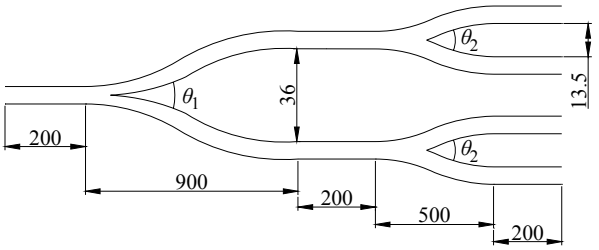

Fig.5 Symmetrical double Y-branch S-bend waveguide

TABLE 1.
STRUCTURE PARAMETER SETTING TABLE OF Y-BRANCH WAVEGUIDE

Y branch waveguide	bending length L/μm	bending height h/μm	branch angle θ
1/2 branch	900	18	2.29°
1/4 branch	500	6.75	1.55°

Substitute two sets of structural parameters in Table 1 into (7) respectively. The transmission lines of 1/2 Y branch waveguide and 1/4 Y branch waveguide are simulated by using MATLAB, as shown in Fig.6 and Fig.7. The degree of bending and smoothness can be vividly seen from the figures.

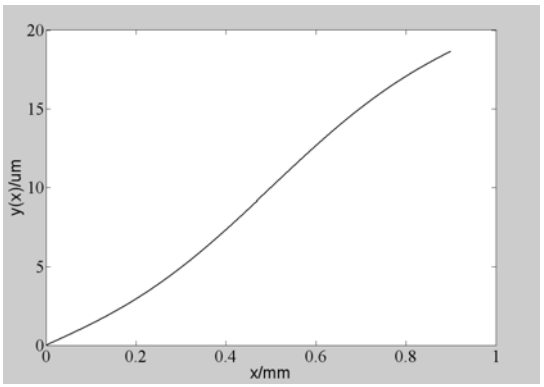

Fig.6 Analog transmission graph of 1/2 Y-branch waveguide

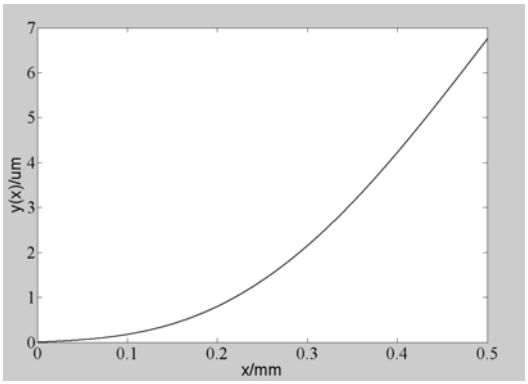

Fig.7 Analog transmission graph of 1/4 Y-branch waveguide

VII. ANALYSIS FOR THE BENDING LOSS OF BRANCH WAVEGUIDE

The bending loss of S-shaped bending increasing arcsine function type waveguide is [5]:

$$\alpha(\mathrm{dB/cm}) \approx \frac{10}{\ln 10} 2\sqrt{2}\pi \frac{h}{L}\frac{C_1}{C_2} \mathrm{e}^{-\gamma}\left(1-\mathrm{e}^{-\frac{\gamma}{2}}\right) \tag{9}$$

where, $\gamma = (C_2 L^2)/(2\pi h)$; C_1 and C_2 have nothing to do with the radius of curvature, and they can be expressed as

$$C_1 = \frac{1}{2Z_C}\frac{\varepsilon_l}{\varepsilon_t},\ C_2 = \frac{2\pi}{\lambda}\frac{(2\Delta N)^{3/2}}{\sqrt{n_b}} \tag{10}$$

where, λ is the wavelength of incident light; n_b is the refractive index of the waveguide cladding; the expression of parameters Z_C, ε_l, ε_t and ΔN are

$$Z_C = \frac{n_b}{2\lambda}\left[w + 2\xi\cos\left(\frac{k_x w}{2}\right)\right]^2 \tag{11}$$

$$\varepsilon_t = \frac{w}{2} + \frac{1}{2k_x}\sin(k_x w) + \xi\cos^2\left(\frac{k_x w}{2}\right),\ \varepsilon_l = \frac{\xi}{2}\cos^2\left(\frac{k_x w}{2}\right)\mathrm{e}^{\frac{w}{\xi}} \tag{12}$$

$$\Delta N = N - n_\mathrm{b} \tag{13}$$

where, N is the effective refractive index of waveguide; w is the width of waveguide; the expression of ξ and k_x are

$$\frac{1}{\xi} = \frac{2\pi}{\lambda}\sqrt{N^2 - n_\mathrm{b}^2},\ k_x = \frac{2\pi}{\lambda}\sqrt{n_\mathrm{e}^2 - N^2} \tag{14}$$

where, n_e is the extraordinary optical refractive index in the waveguide.

The width of waveguide is designed to w=6μm; the wavelength of incident light is λ=1.55μm; the refractive index of waveguide cladding is n_b=1.49; the effective refractive index of waveguide is N=1.50. Substitute the above structural parameters into (9). Calculate the bending loss and length of bending waveguide of 1/2 Y branch waveguide and 1/4 Y branch waveguide, and their expressions are

$$\alpha_1 = 10456.04\mathrm{e}^{-8.3\times10^{-5}L^2}\left(1-\mathrm{e}^{-4.15\times10^{-5}L^2}\right) \tag{15}$$

and

$$\alpha_2 = 3921.02\mathrm{e}^{-2.2\times10^{-4}L^2}\left(1-\mathrm{e}^{-1.1\times10^{-4}L^2}\right) \tag{16}$$

The variation of the bending loss changing with the length of bending waveguide represented by (15) and (16) is programmed and simulated by MATLAB, the simulation results are as follows.

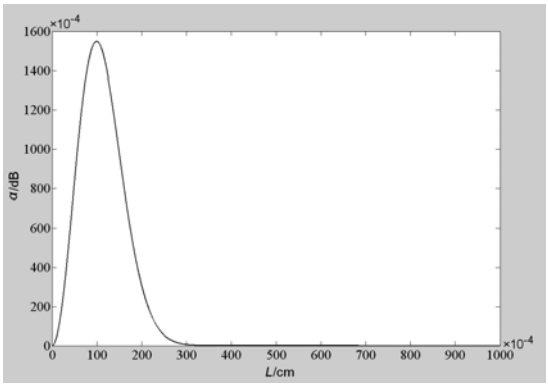

Fig.8 The changes of 1/2 Y-branch waveguide bending loss with length

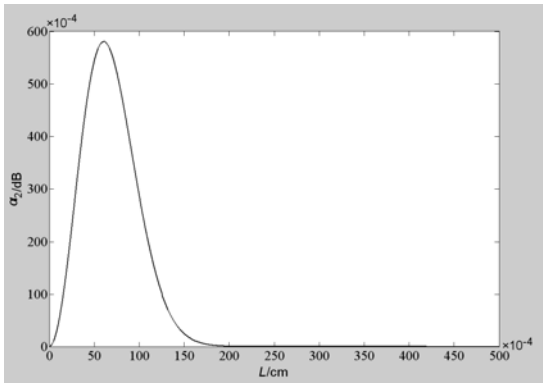

Fig.9 The changes of 1/4 Y-branch waveguide bending loss with length

It can be seen from Fig.8 and Fig.9 that the maximum bending loss of 1/2 Y branch waveguide is the 0.156dB, and the bending loss is close to 0 after L>320μm; the maximum bending loss of 1/4 Y branch waveguide is 0.058dB, and the bending loss is close to 0 after L>200μm. Thus, the double Y branch designed achieves the low-loss requirement.

VIII. Analysis for the Optical Power Conversion in 3dB Coupler

A Y-shaped beam splitter can separate optical power from an input to two branches, or merge optical power from two branch waveguides. 3dB coupler is a passive device to achieve this function. It can be known that the coupling length L generates 100% power transfer depends on the coupling coefficient and the difference of propagation constant between two modes. Under the phase-matching condition ($\delta\approx0$), $L=\pi/2K$. When the length of coupling parts of the two optical waveguides l is half of the coupling length L that achieves 100% power transfer, i.e. $L=\pi/4K$, the power will be evenly distributed at the output. Then the directional coupler is called 3dB coupler, and its structure is shown in Fig.10. 3dB coupler is a special directional coupler, and its Y branch has the dual functions of power distribution and power synthesis.

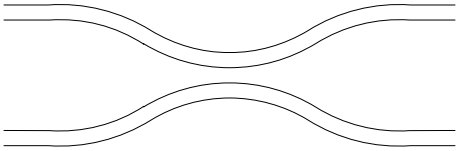

Fig.10 The structure diagram of 3dB coupler

The optical power conversion process of the upper and lower branch waveguide of 3dB coupler in the transmission distance range of 0 to 1.5π under phase-matching condition is simulated by MATLAB, and the simulation result is shown in Fig.11.

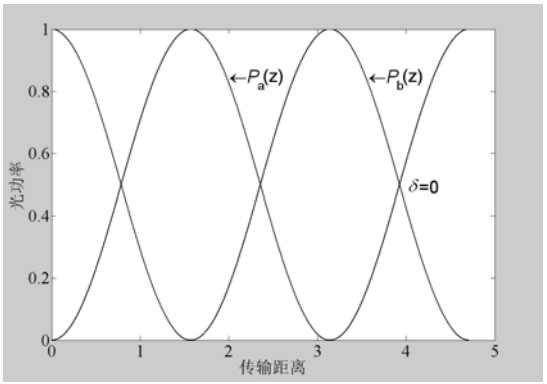

Fig.11 The optical power conversion graph of branch waveguides in 3dB coupler

It can be seen from Fig.11 that under the condition $\delta\approx0$, when the transmission distance is $L=\pi/2K$, the input energy of waveguide b completely converts into the waveguide a.

IX. Production of $LiNbO_3$ Optical Waveguide

When producing the $LiNbO_3$ optical waveguide, the required laboratory air cleanliness is up to 100 degree, i.e. the number of the particles with the diameter larger than 0.5μm per cubic meter should be less than 3500[6]. In addition, the requirements for laboratory temperature and humidity are more stringent. Therefore, the production of $LiNbO_3$ optical waveguide is a time-consuming, high demanding environment and equipment production process.

There are a variety of methods to produce $LiNbO_3$ optical waveguide, such as sputtering method, solution deposition method, epitaxial growth method, Ti diffusion method and annealed proton exchange method. Early Ti diffusion method is more used, and now the annealed proton exchange method is commonly used, because it has some advantages over Ti diffusion method.

A. Comparison of Proton Exchange and Ti Diffusion Technology

Ti diffusion technology and proton exchange method are usually used to produce $LiNbO_3$ optical waveguide. At the early stage of researching $LiNbO_3$ crystal, titanium diffusion is the main way of making optical waveguide. Since 1982 Jackel and others who proposed using proton exchange method to produce optical waveguide, the

method is widely used, and products and devices with good performance are produced.

Titanium diffusion process is as follows: First, rubber coating, photolithography, coating film, stripping should be carried out on the surface of $LiNbO_3$ crystal to form optical waveguide titanium strip; and then it should be diffused in high temperature diffusion furnace for about 8~10h at about 1025℃ to form optical waveguide with the refractive index of Gaussian distribution. Proton exchange process is as follows: After coating film, lithography, corrosion, removing the metal film with the shape of the waveguide, the sample is put to the acid solution to carry out proton exchange to form a high refractive index optical waveguide; and then it is annealed at high temperature heater, followed by grinding and polishing, and then the final high-quality optical waveguide is formed.

Compared to titanium diffusion, the most important advantage of proton exchange is that the anti-light damage of proton exchange optical waveguide is better than that of titanium diffusion optical waveguide because hydrogen ions can reduce the light damage of $LiNbO_3$ crystal. The anti-light damage of proton exchange optical waveguide is unexpectedly increased, reaching three orders of magnitude. About one order of magnitude of the increase is due to the decrease caused by electro-optic coefficient, which plays a key role in the light damage of $LiNbO_3$ crystals. Even after strong annealing and making the electro-optic coefficient of the crystal fully restore to the level of unexchanged crystal, the light damage of proton exchange optical waveguide is one order higher than that of crystals with the same composition. An important reason for the better anti-light damage ability of proton exchange optical waveguide is that the proton exchange will cause strong oxidation of iron ions in the crystal. In addition, researchers found that the dark conductivity of proton exchange optical waveguide significantly increases, which is another important reason for its significant improvement of anti-light damage ability [7].

Based on the above advantages, proton exchange method is used to produce strip waveguides on $LiNbO_3$ substrate of three-component acceleration seismic geophones.

Note that the proton exchange method is only suitable for the production of X-cut and Z-cut $LiNbO_3$ waveguide, not suitable for the production of Y-cut $LiNbO_3$ crystal, because benzoic acid will corrode the Y- surface of $LiNbO_3$ crystal.

B. Proton Exchange

After coating film, lithography and etching, proton exchange annealing process can be carried on the $LiNbO_3$ substrate, and thus the optical waveguides are formed. The formation of optical waveguides can be divided into two phases: the basic proton exchange of organic proton source and annealing treatment.

Proton exchange temperature is 245℃; the exchange time is 3.5~4h; and the temperature error controls within ±0.5℃. Benzoic acid with a purity of 99.99% is used as the proton exchange source, and a certain amount of benzoic acid lithium diluent is added. The structure of the proton exchange furnace is shown in Fig.12, which is made from glass tubes. Benzoic acid is heated to the desired exchange temperature, then the substrate is added. When the exchange is completed, first cleaning, then slowly put into the annealing furnace with the oxygen atmosphere for annealing process. Annealing temperature and annealing time respectively are 350℃ and 4h; the temperature error controls within ±1.0℃; and the rate of inputting oxygen is 2~3L per minute.

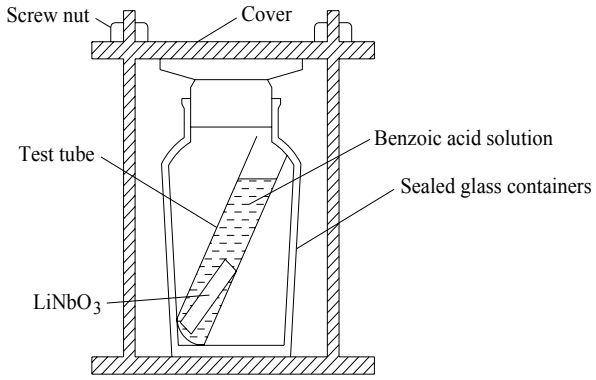

Fig.12 Proton exchange device

When the hydrogen atom lose electron, it becomes protons. So the proton exchange process is essentially ion exchange process, i.e., Li^+ in $LiNbO_3$ crystal is replaced by H^+ in acid. If strong acid (H_2SO_4, $HNbO_3$) is used as the proton source, because of its high concentration of H^+, Li^+ in $LiNbO_3$ is almost completely exchanged into $HNbO_3$, which completely changes the structure of $LiNbO_3$ crystal. If weak acid (benzoic acid, phosphoric acid, etc.) is used for the exchange source, then parts will be exchanged to replace Li^+, which will not change the main structure of $LiNbO_3$ X-cut and Z-cut $LiNbO_3$ wafers can use benzoic acid for proton exchange. Z-cut $LiNbO_3$ wafer is used in the designs.

Benzoic acid is commonly used as the proton exchange source, because its production process is relatively mature, and there is a suitable operating temperature range, in which it will not decompose in the exchange. And its acid is weaker compared with other acid, which does less harm to the material. The diffusion constant and activation energy values of methyl benzoate acid and benzoic acid solution in the temperature range are shown in Table 2 [8].

TABLE 2.
PARAMETERS CHANGES OF TWO KINDS OF ACID AT DIFFERENT TEMPERATURE RANGES

Acid solution	Methyl benzoate acid	Benzoate acid
Temperature range (°C)	109−263	122−249
Diffusion constant D_0 (μm_2 /hr)	7.02·107	7.36·109
Activation energy Q (kJ/mol)	75.58	94

The chemical expressions of proton exchange are

$$C_6H_5COOH \leftrightarrow C_6H_5COO^- + H^+ \quad (17)$$

$$LiNbO_3 + xH^+ \leftrightarrow Li_{1-x}H_xNbO_3 + xLi^+ \quad (18)$$

Proton exchange time is determined by the thickness of optical waveguide. When carrying out high-temperature exchange on Z-cut $LiNbO_3$ crystal used by the design, the time and temperature should be well controlled to prevent its rupture.

C. Annealing

The purpose of annealing is to reduce the concentration of H^+ in the crystal, then Δn_e is reduced, and the depth of optical waveguide becomes deeper, so that the distribution of refractive index changes from a step-gradient type to gradual change, which reduces the transmission loss of optical waveguide, and greatly restores electro-optic coefficient and the nonlinear coefficient. Annealing requires high temperature constant temperature heater. The annealing time is from minutes to hours; the annealing temperature is 300~400℃; and the diffusion depth d_a of the concentration of H^+ after annealing meets

$$d_a = 2\sqrt{D_a(T)t_a} \quad (19)$$

where, t_a is the annealing time; D_a is the diffusion coefficient of the annealing process.

Set the distribution of H^+ after proton exchange be a rectangular plate with the thickness d_e and the height Ax_e. x_e represents the concentration coefficient of H^+ after proton exchange, and A is the atomic density coefficient of $LiNbO_3$. Assuming the total amount of H^+ is the same after annealing, and then the concentration of H^+ $C_H(y, t_a)$ after annealing can be expressed by the error function $\mathrm{erf}(x) = \frac{2}{\sqrt{\pi}}\int_0^x \exp(-t^2)dt$ as

$$C_H(y,t_a) = \frac{Ax_e}{2}[\mathrm{erf}(\frac{d_e + y}{d_a}) + \mathrm{erf}(\frac{d_e - y}{d_a})] \quad (20)$$

With the increase in the degree of annealing, the concentration of H^+ on the surface of $LiNbO_3$ crystal decreases and its expression is

$$C_H(0,t_a) = Ax_e\mathrm{erf}(\frac{d_e}{d_a}) = Ax_a \quad (21)$$

Where, x_a is the concentration coefficient of H^+ after annealing.

Eqution (21) can be approximates as

$$C_H(y,t_a) = \frac{2Ax_ed_e}{\sqrt{\pi}d_a}\exp(\frac{-y^2}{d_a^2}) = Ax_a\exp(\frac{-y^2}{d_a^2}) \quad (22)$$

It can be obtained from (22) that

$$x_a = \frac{2x_ed_e}{\sqrt{\pi}d_a} \Rightarrow \frac{d_a}{d_e} = \frac{2x_e}{\sqrt{\pi}x_a} \quad (23)$$

In the α phase region, $x_a \le 0.12$, $x_e \approx 0.8$. Substitute them into (23). If want to reach α-phase area after annealing, the required condition is

$$d_a \ge 7.5d_e \quad (24)$$

where d_e is the depth of optical waveguide after proton exchange; d_a is the depth of optical waveguide after annealing.

By analyzing and comparing the data, a better proton exchange and annealing condition is arrived: the width of $LiNbO_3$ optical waveguide designed is w=6μm; the proton exchange condition is $T_e = 245$ ℃, $t_e = 3.5 \sim 4$ h; the annealing condition after proton exchange is $T_a = 350$ ℃, $t_a = 4$ h. High-quality $LiNbO_3$ optical waveguide is obtained in the above conditions.

X. CONCLUSIONS

A right and rational design of sensitive element of three-component acceleration seismic geophone dual M-Z interferometer is quite vital to the correct detection of acceleration by three-component acceleration seismic geophone. While the Y branch waveguide the basic optical components composed of dual M-Z interferometer. Therefore, the design of the Y branch waveguide directly affects the performance of three-component acceleration seismic geophone.

The symmetry double Y branch waveguide of dual M-Z interferometer and 3dB coupler used for an optical power sharing are designed. The bending loss of branch waveguide is analyzed and calculated. The transmission and the bending loss changing with the length is simulated. The branch waveguide designed based on the above method has the advantage of low loss.

ACKNOWLEDGEMENTS

This paper is supported by the followings: National Natural Science Foundation of China (41074090), Key Technologies R & D Program of Henan Province (022102210360), Control Engineering Key Discipline Open Foundation Program of Henan Province (KG2009-12), and Science Research Priorities Program of Henan Educational Committee (2009B4800004).

REFERENCES

[1] Guo Wenbin, Wang Lizhi, Liu Caixia, Ruan Shengping, Chen Weiyou, The study of transmission characteristics of a 1717 all fluorinated polyimide arrayed waveguide grating multiplexer, 2011 Symposium on Photonics and Optoelectronics, Symposium on Photonics and Optoelectronics, SOPO 2011.

[2] Yi Zhangjing, Yan Rongjin, Erickson Timothy A., Safaisini Rashid, Lear Kevin L., Optimization of waveguide structure for local evanescent field shift detection, Proceedings of SPIE−The International Society for Optical Engineering, v7941, 2011, Integrated Optics: Devices, Materials, and Technologies XV.

[3] Bozzi M., Georgiadis A., Wu K., Review of substrate-integrated waveguide circuits and antennas, IET

Microwaves, Antennas and Propagation, v 5, n 8, p 909-920, 06 June 2011.
[4] Bamiedakis N., Penty R.V., White I.H., Hutter T., Ellliott S.R., Low-cost PCB-integrated polymer waveguide sensor for gas detection, 2011 Conference on Lasers and Electro-Optics: Laser Science to Photonic Applications, Conference on Lasers and Electro-Optics: Laser Science to Photonic Applications, CLEO 2011.
[5] Alhzzoury A. Ismail, Raveu N., Prigent G., Pigaglio O., Baudrand H., Al-Abdullah K., Substrate integrated waveguide filter design with wave concept iterative procedure, Microwave and Optical Technology Letters, v53, n12, p2939-2942, December 2011.
[6] Hu Shuai, Liu Fang, Wan Ruiyuan, Huang Yidong, Coupling characteristics between slot plasmonic mode and dielectric waveguide mode, Proceedings of SPIE−The International Society for Optical Engineering, v7990, 2011, Optical Sensors and Biophotonics II.
[7] Liu Fang, Li Yunxiang, Wan Ruiyuan, Huang Yidong, Feng Xue, Zhang Wei, Hybrid coupling between long-range surface plasmon polariton mode and dielectric waveguide mode, Journal of Lightwave Technology, v29, n9, p1265-1273, 2011.
[8] Lang Tingting, Lin Xufeng, He Jianjun, Fabrication of silica-on-silicon arrayed waveguide gratings, Guangxue Xuebao/Acta Optica Sinica, v31, n2, p0213003, February 2011 Language: Chinese.

De En, born in Tongliao, Inner Mongolia Province, 1962, Doctor of physical electronics, institute of precision instrument and optoelectronics engineering, Tianjin University, Tianjin, China, 2006. His work focuses on photoelectron technology and modern sensing technology. Prof. En completed five national and provincial key projects, and won five national patents.

Jieyu Feng, born in Anyang, Henan Province, 1985, Master of control theory and control engineering, school of electrical engineering and automation, Henan Polytechnic University, Jiaozuo, China, 2012.

Ningbo Zhang, born in Jiyuan, Henan Province, 1987, Master of control theory and control engineering, School of Electrical Engineering and Automation, Henan Polytechnic University, Jiaozuo, China, 2012.